

## Kiglapait mineralogy V: Feldspars in a hot, dry magma

S.A. MORSE<sup>1,\*</sup>

<sup>1</sup>Department of Geosciences, University of Massachusetts, 611 North Pleasant Street, Amherst, Massachusetts, 01003-9297, U.S.A.

### ABSTRACT

The lithology of the 1.305 Ga Kiglapait intrusion is dominated by a Lower Zone of troctolite, succeeded by an Upper Zone of olivine gabbro, ferrodiorite, and syenite with olivine composition of pure fayalite. The feldspar composition of the intrusion varies from An<sub>68</sub> to An<sub>9</sub> over a thickness of 8.4 km from the base to a sandwich horizon under an Upper Border Zone. The anhydrous nature of the Kiglapait syenites is shown by their high temperature, by the loss of minor biotite up-stratigraphy in the intrusion, and the absence of amphibole. The end-stage feldspar of the Kiglapait syenites is that of a solidus embedded in a solvus in a 3 kbar eutectic at 1000 °C. The end-member assemblage at temperature and pressure is invariant. The final bulk composition is relatively An-rich—An ~11%—with a composition of  $X_{Or} = 1/3$  when projected to the Ab-Or sideline. The experimental feldspar solvus when corrected for the effects of An and Ba and referred to 3 kbar penetrates the solidus and fits the experimental tie lines. These conditions precede a stage of local coarsening under subsolidus conditions that is found in colloform symplectites invading mesoperthite. The oligoclase-orthoclase symplectites are iso-compositional with their host mesoperthites. The coarsening is assumed to be related to a plausibly F-rich vapor phase that is locally consumed with time. The observed phase compositions indicate the end of exsolution at ~800 °C at 3 kbar on the binodal solvus.

**Keywords:** Feldspar compositions, Kiglapait Intrusion, chemistry, textures, exsolution, symplectite, coarsening, solvus, syenites, cooling history

### INTRODUCTION

N.L. Bowen (1945) noticed that pure albite would never occur in the presence of calcium, in what became known as the “plagioclase effect.” By that time he must have realized that his (1915) bending of the plagioclase–diopside field boundary to pure Ab was a mistake, and if he had lived long enough to learn about linear partitioning he would have discovered that the plagioclase in equilibrium with the multicomponent liquid lying on the Di-Ab sideline was of composition An<sub>9</sub> (Morse 1997). This principle of the role of calcium, along with the presence of fayalite, has a profound effect on the endpoint of ternary feldspar crystallization at anhydrous pressure.

The classic story of H<sub>2</sub>O-saturated or -bearing ternary feldspars begins with Tuttle and Bowen (1958, submitted 1954) and flows through Yoder et al. (1957), Stewart and Roseboom (1962; in part via J.B. Thompson), Morse (1969b, 1970), Fuhrman and Lindsley (1988), to the masterful study of Nekvasil and Lindsley (1990), and a generation of work by Ian Parsons and his colleagues (e.g., 2015), in particular with the late W.L. Brown.

This work shows that in the Kiglapait intrusion the endpoint of extreme fractional crystallization of a troctolitic parent magma is composed of a ferrosyenite making an azeotrope with bulk composition An<sub>11</sub>,  $X_{Or} = 1/3$  embedded in a solvus with paired limits at Or<sub>21</sub> and Or<sub>52</sub> as projected from An onto the Ab-Or sideline. The locally arrested symplectite intergrowths on mesoperthite were exsolved in the subsolidus to ~800 °C.

The low-pressure solvus determined for a Ca-bearing Kiglapait mesoperthite (Morse 1969b) has the same form as in the solvus at 5 kbar in the system Ab-Or-H<sub>2</sub>O of Morse (1970) and that of Waldbaum and Thompson (1969). When adjusted for Ba content, An content and pressure from published literature studies it matches closely the 3 kbar Kiglapait endpoint determined from experimental studies. The effect of fayalite on plagioclase compositions (Morse and Brady 2017b) is striking in its ability to lower the temperatures of crystallization, in effect doing the work of water on crystallization temperatures without affecting the role of calcic pyroxene in maintaining relatively high An contents of the liquids compared with the very low An-contents of hydrous ternary feldspar liquids.

### Previous work

The first and fundamental report on the Kiglapait feldspars was the crystallographic study of Speer and Ribbe (1973). This paper is important for several reasons. It was based mainly on new sampling in the Kiglapait intrusion by Speer, especially in the southern to middle part of the intrusion. It showed that the oligoclase component of mesoperthite was metastably monoclinic, coexisting with a monoclinic orthoclase component, and therefore showing that the original mesoperthite crystal was a sodium-rich monoclinic sanidine. It also located a bulk composition of mesoperthite near or at the Na limit, furnishing a practical boundary for the existence of mesoperthite. This was also the first study on Kiglapait feldspars to show a ternary crystallization path. Additional reports were made on potassium and rubidium by Morse (1981a), strontium (Morse 1981b), and the experimental partitioning of Sr and Ba (Morse and Allaz 2013).

\* E-mail: tm@geo.umass.edu

### Geologic setting of the Kiglapait Intrusion

The 1.305 Ga Kiglapait layered intrusion is located on the north coast of Labrador (Fig. 1), miraculously preserved among nine slightly older troctolitic bodies of the Nain Plutonic Suite (Ryan 1990). Most of the igneous bodies in this suite are anorthosites, generally with pale hypersthene (noritic) varieties to the West, and darker olivine (troctolitic) varieties to the East (Morse 2015b; Xue and Morse 1993). The intrusion (Morse 1969a and online; Morse 2015b) is oval, about 32 km long North to South and 26 km wide, West to East (Fig. 1). Its topography is dominated by a chain of sharp-peaked, 1 km high mountains rising from the sea to the north (the Kiglapait Mountains) and from Medusa Bay to the South (Mt. Thoresby).

The entire bowl within the mountains shows convergent layers of troctolite, olivine gabbro, titanomagnetite gabbro, fluorapatite ferromonzonite, and ferrosyenite culminating at the base of an Upper Border Zone that contains the entire stratigraphy of the Layered Series in reverse stratigraphic order, from the most Mg-rich olivine to pure fayalite at the sandwich horizon (Fig. 1). The map shows well-preserved contact rocks of two metamorphic suites—the Snyder and Falls Brook Groups—at the northwest; these have been used to infer the pressure of intrusion at the present erosion level, as ~2.8 kbar (Berg and Docka 1983).

The intrusion is composed of an Inner Border Zone of coarse but quenched olivine gabbro, followed upward by a very thick Lower Zone of troctolite, successively overlain by olivine gabbro (incoming cumulus augite marking the base of the Upper Zone), followed by the succession noted above. Three major sampling traverses are located on the map: Sally Lake (SL) to the North, David-Billy (DB) in the middle, and Caplin-Patsy (CP) in the South on the almost continuous exposures along Port Manvers Run. Further information on the intrusion and its petrography and chemistry is summarized in Morse (2015b).

An enlarged sketch map of the central area of the intrusion (Fig. 2) illustrates the locations of zone and subzone boundaries defining mineral and rock types, and the nature of the Upper Border Zone. Detailed maps of sample locations are available in the Supplementary Material<sup>1</sup> of this paper.

### MAGMATIC PRESSURE

The pressure history of the crystallizing Kiglapait magma is an important consideration in the experimental investigation. We may take the sanidinite-facies contact estimate of 2.8 kbar (Berg and Docka 1983) as appropriate to the current exposure level at the top of the Upper Border Zone and round it to 3 kbar. Using the modified PREM table of Stacey and Davis (2009) for crustal pressures we then find a value for the original Kiglapait roof of 9.6 km depth (Morse 2014). For an original *magma* depth of 8400 m (Morse 1969a) we find the model initial pressure at the base to be ~5 kbar. Just above the Upper Zone boundary the pressure is 3.6 kbar at a magma depth of 3000 m, and the end of crystallization occurs at 2.8 kbar. For experimental purposes with the piston-cylinder apparatus, a standard pressure of 5 kbar was used.

This protocol was used for the previous study of the Lower Zone (Morse et al. 2004) and extended to the Upper Zone by Peterson (1999). In a study of Upper Zone thermal history, experiments were also made at  $P = 3$  kbar (Morse and Brady 2017a).

### WATER CONTENT OF THE INTRUSION

Since the work of Huntington (1979) students of the Nain Plutonic Suite (NPS) have been convinced that the Kiglapait intrusion was very dry. The principal carrier of volatile components in the intrusion is apatite (Huntington 1979). The abundance of fluorine rises with fractionation, whereas the inferred OH component falls to zero. The hydrous phase in the intrusion of any consequence is red oxy-biotite (Fig. 3). The data of Huntington show a dramatic decrease in modal biotite toward the end of crystallization ending at zero. The absence of amphibole is also a key to the low activity of water in the intrusion.

None of the 10 troctolitic intrusions of the NPS have shown signs of significant H<sub>2</sub>O content; their marginal contacts tend to be dry gneisses; their associated anorthosites are dry dark olivine-bearing bodies and pale orthopyroxene bodies. One contact zone of the latter contains osumilite, the OH-free version of cordierite (Berg 1977) and other dry granulites are the hallmark of the wall rocks.

### WET CHEMICAL ANALYSES

Bulk compositions of Kiglapait feldspars were procured by wet chemical analysis, which has the advantage of giving separate values for the iron oxides and furnishing records of stoichiometry. The 29 Kiglapait feldspar specimens chosen for bulk chemical analysis were each separated from the crushed rock sized 75–180  $\mu\text{m}$  in stainless steel sieves. They were then floated in bromoform, washed with methanol and acetone, and separated on a magnetic separator to remove any further mafic mineral fragments. Typical settings on the separator were 1.4 A with a 5° tilt, with the feldspar collected on the non-magnetic side. Nine samples showing minor rusty weathering were leached from 3 to 9 h in dilute nitric acid to remove any coating (these are samples with serial numbers 12, 14, 20, and 24–29 in Table 1). Analyses are listed (Table 1) in stratigraphic order, with stratigraphic height given as volume percent solidified (PCS), the remaining fraction of liquid ( $F_L$ ) and traverse identified. In 11 cases, there were duplicate or triplicate analyses. Because no systematic bias was detected among the analyses, multiple analyses were averaged.

Samples at and above 99.90 PCS were found to contain percent-scale values of BaO and those were quantified. Further analyses for Ba in lines 1–18 were conducted by XRF at the University of Massachusetts.

Cation values for 8 O atoms are listed in Table 2. The alkalis are reasonably balanced by the Si content less 2. The detailed distribution of the reduced alkali–silica balance is about the ideal value of zero; the scatter is contained within about  $\pm 0.06$  cation units in the balance. The alumina balance against the divalent cations Ca and Ba is generally excellent. A slightly better correlation is obtained when Fe, Mg, and Ti are considered, possibly signaling some tetrahedral occupancy of Fe<sup>2+</sup>. The ferrous fraction (relative to ferrous + ferric iron) of feldspar is shown (Fig. 4) to grow generally with stratigraphic height in the intrusion until the Main Ore Band, after which it decreases and then increases again.

<sup>1</sup>Deposit item AM-17-106098, Supplementary Material. Deposit items are free to all readers and found on the MSA web site, via the specific issue's Table of Contents (go to [http://www.minsocam.org/MSA/AmMin/TOC/2017/Oct2017\\_data/Oct2017\\_data.html](http://www.minsocam.org/MSA/AmMin/TOC/2017/Oct2017_data/Oct2017_data.html)).

### ELECTRON MICROPROBE DETERMINATIONS

Most electron probe determinations were made on polished grain mounts of cleavage flakes embedded in epoxy, hence with a cleavage frequency approximately equal between (001) and (010). They were made by rapid analysis, determining only An, Ab, and Or on  $\geq 10$  flakes per sample with a precision (Morse 1978) of 1 SD =  $\pm 0.84\%$  An in the range  $An_{15}$ – $An_{51}$ , which includes antiperthites and mesoperthites previously analyzed by wet chemistry. This procedure was designed to find the range and mean of An contents in a given sample. Analyses were made with voltage set at 15 kV, 15 nA, with a beam diameter of 15–20  $\mu\text{m}$  to capture fine-scale feldspar intergrowths, and a counting time of 15 s. The method is useful because it represents

a large sample size, typically several hundred grams of drill core (Morse 2012). All analyses were monitored routinely by reference to standard plagioclase PG-721. By this means 192 separated feldspar samples were analyzed, ranging from  $An_{67}$  to  $An_{8.7}$ . The observed “An range” in a given sample was used to estimate the volume of trapped liquid (Morse 2012).

Polished thin sections and experimental charges were analyzed with the same settings as above for voltage and current and time, but with beam size typically at 2  $\mu\text{m}$  for feldspar. For experimental glass, the beam diameter was set at 10  $\mu\text{m}$  and for mafic minerals 1  $\mu\text{m}$ . For alkali feldspars near the mesoperthite composition, five samples were analyzed in polished thin section to constrain the origin of oligoclase-orthoclase symplectites.

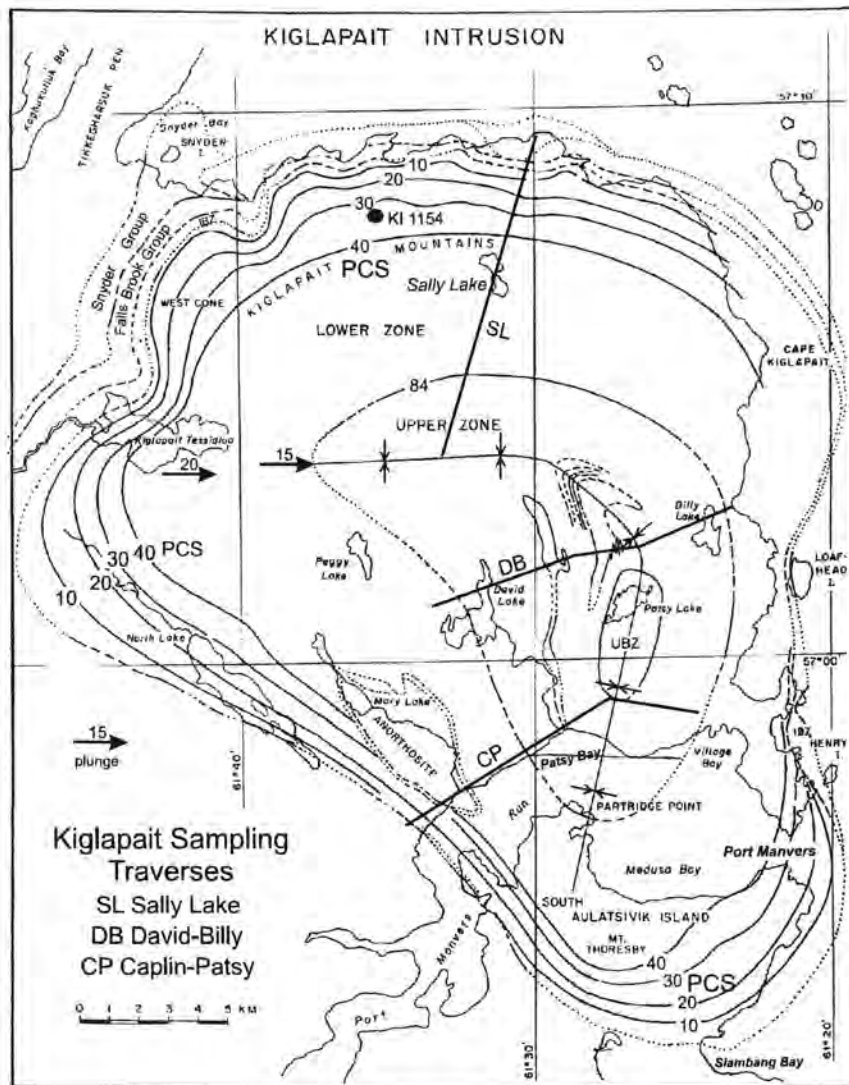


**FIGURE 1.** Sketch map of the Kiglapait Intrusion with three sampling traverses (see heading title) and one off-traverse sample location (KI 1154) to locate the samples with bulk compositions determined by wet chemistry in this paper (Tables 1 and 2). The contours are those of volume percent solidified (PCS) and are based on the strike of layering and the volumes of 13 cross sections described in the original Memoir (Morse 1969a). Plunge values of layering are shown in the western part of the synclinal axis, these show shallowing plunges limiting the probability that the steepness of layering has increased during subsidence: the layering seen must have been within 15° of the present dip. Abbreviations: UBZ = Upper Border Zone; IBZ = Inner Border Zone. Larger-scale maps with feldspar sample locations are shown in the Supplementary Material<sup>1</sup>.

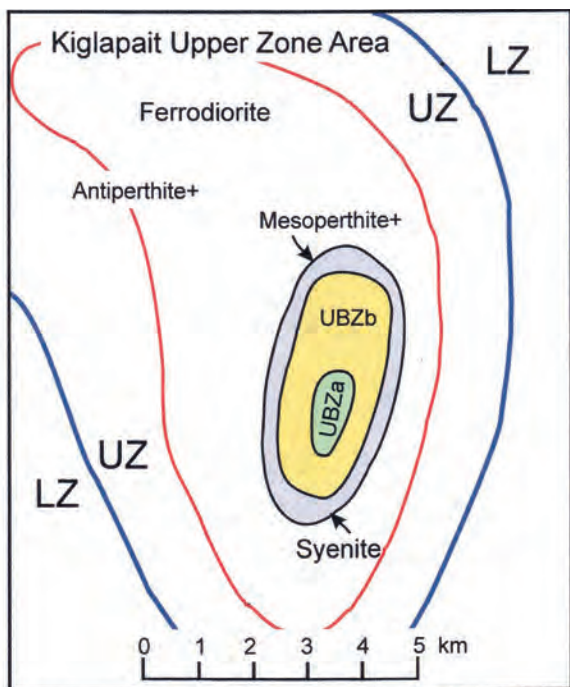


FIGURE 2. Sketch map of the Upper Zone area of the Kiglapait Intrusion showing the LZ-UZ boundary, the contours of antiperthite+ and mesoperthite+, and the two divisions of the Upper Border Zone. UBZa is the LZ equivalent with primitive mineral compositions at the top and more evolved ones below, and UBZb is the Upper Zone equivalent terminating in a sandwich horizon at the top of the syenite. (Color online).

FELDSPAR COMPOSITION SPACE

Stratigraphic variation of plagioclase composition

The feldspar composition range in the Kiglapait intrusion is shown in Figure 5 plotted against stratigraphic height expressed as  $-\log F_L$  and as PCS. The “assumed cumulus model” favors the higher An values so as to best represent the results of the liquid path, whereas the accompanying lower values of An are shown to represent the trapped liquid effect as measured by the An range in the sample and the resulting estimate of the residual

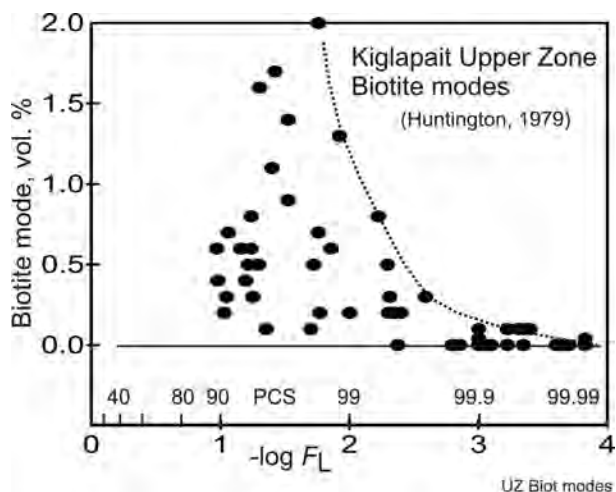


FIGURE 3. Biotite mode in the Upper Zone of the Kiglapait intrusion. The decline above ~98 PCS clearly indicates that biotite and its water are not conserved components of the intrusion.

TABLE 1. Kiglapait feldspars in stratigraphic order: Wet chemical analyses

Series no.	KI SPLNO	Traverse		C <sub>p</sub>	Weight percent												Sum	Anl.
		PCS	F(L)		SiO <sub>2</sub>	TiO <sub>2</sub>	Al <sub>2</sub> O <sub>3</sub>	Fe <sub>2</sub> O <sub>3</sub>	FeO	MgO	CaO	Na <sub>2</sub> O	K <sub>2</sub> O	BaO				
1	KI 3223	15.00	0.850	C <sub>p</sub>	51.45	0.05	30.38	0.33	0.24	0.09	12.95	4.12	0.19	0.012	99.81	123		
2	KI 1154	32.00	0.680	NC	51.62	0.12	29.94	0.66	0.28	0.29	12.59	4.04	0.16	0.014	99.71	Wiik		
3	KI 2008	35.00	0.650	C.Kig	52.08	0.10	28.96	0.27	0.36	0.34	12.82	3.76	0.24	nd*	98.93	Wiik		
4	KI 3230	39.00	0.610	C <sub>p</sub>	52.72	0.07	29.51	0.26	0.28	0.14	11.94	4.62	0.27	0.016	99.83	123		
5	KI 3645	51.80	0.482	SL	51.37	0.08	30.63	0.25	0.15	0.14	13.17	3.73	0.21	nd	99.73	2		
6	KI 3276	68.00	0.320	C <sub>p</sub>	53.84	0.06	28.76	0.35	0.33	0.16	11.17	5.08	0.27	0.019	100.04	123		
7	KI 3360	80.00	0.200	C <sub>p</sub>	53.63	0.05	29.28	0.15	0.28	0.02	11.07	5.11	0.26	0.018	99.87	12		
8	KI 3362	83.00	0.170	C <sub>p</sub>	54.26	0.07	28.83	0.18	0.27	0.16	10.51	5.44	0.24	0.02	99.98	123		
9	KI 3363	84.50	0.155	C <sub>p</sub>	54.59	0.06	28.56	0.11	0.30	0.15	10.40	5.51	0.25	0.02	99.95	123		
10	KI 3367	87.00	0.130	C <sub>p</sub>	55.19	0.10	28.31	0.04	0.19	0.08	9.85	5.23	0.29	0.02	99.30	2		
11	KI 3369	89.30	0.107	C <sub>p</sub>	55.74	0.08	27.71	0.03	0.25	0.06	9.55	5.64	0.34	0.026	99.43	2		
12	KI 3345	93.00	0.070	DB	57.30	0.07	26.78	0.04	0.20	0.04	8.40	5.84	0.59	nd	99.26	2		
13	KI 3243	93.70	0.063	DB	57.48	0.12	26.91	0.04	0.31	0.12	8.19	6.09	0.46	nd	99.72	2		
14	KI 3347	93.90	0.061	DB	58.33	0.08	26.39	0.07	0.11	0.06	7.52	6.50	0.59	0.039	99.69	2		
15	KI 3377	97.00	0.030	C <sub>p</sub>	58.94	0.04	25.48	0.16	0.40	0.07	6.81	7.22	0.78	nd	99.90	123		
16	KI 3002	97.50	0.025	C <sub>p</sub>	59.38	0.09	24.40	0.23	0.29	0.00	6.22	7.68	1.02	0.116	99.43	2		
17	KI 3379	98.60	0.014	C <sub>p</sub>	60.57	0.06	24.31	0.20	0.23	0.03	5.49	7.82	1.26	0.148	100.12	123		
18	KI 3009	99.50	0.005	C <sub>p</sub>	60.89	0.03	23.25	0.29	0.35	0.02	5.07	8.09	1.42	0.248	99.66	13		
19	KI 4119	99.60	0.004	C <sub>p</sub>	61.64	0.05	23.72	0.01	0.27	0.02	4.93	7.43	1.28	nd	99.35	2		
20	KI 4079	99.90	0.001	C <sub>p</sub>	63.17	0.05	22.12	0.02	0.21	0.00	2.73	7.41	3.32	0.91	99.94	2		
21	KI 4061	99.94	0.001	C <sub>p</sub>	62.59	0.08	23.01	0.03	0.30	0.01	3.53	7.44	2.47	1.02	100.48	2		
22	KI 4081	99.94	0.001	C <sub>p</sub>	63.34	0.06	21.25	0.04	0.37	0.01	1.89	6.44	4.76	1.42	99.58	2		
23	KI 3001	99.97	0.0003	C <sub>p</sub>	63.26	0.00	21.17	0.05	0.12	0.00	1.71	7.14	5.49	1.30	100.24	12		
24	KI 4106	99.97	0.0003	C <sub>p</sub>	63.45	0.04	21.58	0.02	0.20	0.00	2.77	6.23	4.75	1.25	100.29	2		
25	KI 4076	99.98	0.0002	C <sub>p</sub>	64.01	0.06	21.32	0.02	0.18	0.00	1.65	6.51	5.30	1.30	100.35	2		
26	KI 3381	99.98	0.0002	C <sub>p</sub>	62.99	0.02	21.95	0.00	0.18	0.01	2.62	7.38	3.96	1.05	100.16	13		
27	KI 4110	99.99	0.0001	C <sub>p</sub>	63.61	0.04	21.27	0.03	0.18	0.00	1.94	5.73	5.52	1.18	99.50	2		
28	KI 4063	99.99	0.0001	C <sub>p</sub>	62.77	0.05	22.21	0.02	0.18	0.01	2.88	6.75	3.95	1.02	99.84	2		
29	KI 4104	99.99	0.0001	DB	63.25	0.04	21.60	0.02	0.16	0.00	2.23	6.54	4.97	1.19	100.00	2		

Notes: nd\* BaO not determined; lines 1–18 by XRF at UMass. C.Kig = Cape Kiglapait. Anl: Analysts: Wiik = H.B. Wiik; 1 = Tadashi Asari; 2 = Ken-ichiro Aoki; 3 = E. Engleman, USGS. Multiple digits represent averages.

**TABLE 2.** Kiglapait feldspars in stratigraphic order: Eight O atoms

SN	SPLNO	Cations										Ternary				
		Si	Ti	Al	Fe3	Fe2	Mg	Ca	Na	K	Ba	SUM	100 XAn	An	Ab	Or
1	KI 3223	2.347	0.002	1.633	0.011	0.009	0.006	0.633	0.364	0.011	0*	5.017	63.5	62.8	36.1	1.1
2	KI 1154	2.356	0.004	1.611	0.023	0.011	0.020	0.616	0.358	0.009	0	5.007	63.3	62.7	36.4	0.9
3	KI 2008	2.392	0.003	1.568	0.009	0.014	0.023	0.631	0.335	0.014	nd*	4.990	65.3	64.4	34.2	1.4
4	KI 3230	2.398	0.002	1.582	0.009	0.011	0.009	0.582	0.407	0.016	0	5.016	58.8	57.9	40.5	1.6
5	KI 3645	2.342	0.003	1.646	0.009	0.006	0.010	0.643	0.330	0.012	nd	4.999	66.1	65.3	33.5	1.2
6	KI 3276	2.439	0.002	1.536	0.012	0.013	0.011	0.542	0.446	0.016	0	5.016	54.9	54.0	44.4	1.6
7	KI 3360	2.431	0.002	1.564	0.005	0.011	0.001	0.538	0.449	0.015	0	5.015	54.5	53.7	44.8	1.5
8	KI 3362	2.453	0.002	1.536	0.006	0.010	0.011	0.509	0.477	0.014	0	5.019	51.6	50.9	47.7	1.4
9	KI 3363	2.467	0.002	1.521	0.004	0.011	0.010	0.504	0.483	0.014	0	5.017	51.1	50.3	48.2	1.4
10	KI 3367	2.499	0.003	1.511	0.001	0.007	0.005	0.478	0.459	0.017	0	4.980	51.0	50.1	48.1	1.8
11	KI 3369	2.522	0.003	1.477	0.001	0.009	0.004	0.463	0.495	0.020	0	4.994	48.3	47.4	50.6	2.0
12	KI 3345	2.585	0.002	1.424	0.001	0.008	0.003	0.406	0.511	0.034	nd	4.973	44.3	42.7	53.7	3.6
13	KI 3243	2.581	0.004	1.424	0.001	0.012	0.008	0.394	0.530	0.026	nd	4.981	42.6	41.5	55.8	2.8
14	KI 3347	2.615	0.003	1.394	0.002	0.004	0.004	0.361	0.565	0.034	0.001	4.983	39.0	37.6	58.9	3.5
15	KI 3377	2.643	0.001	1.347	0.005	0.015	0.005	0.327	0.628	0.045	nd	5.016	34.3	32.7	62.8	4.5
16	KI 3002	2.679	0.003	1.298	0.008	0.011	0.000	0.301	0.672	0.059	0.002	5.030	30.9	29.2	65.1	5.7
17	KI 3379	2.708	0.002	1.281	0.007	0.009	0.002	0.263	0.678	0.072	0.003	5.021	28.0	26.0	66.9	7.1
18	KI 3009	2.740	0.001	1.233	0.010	0.013	0.001	0.244	0.706	0.082	0.004	5.031	25.7	23.7	68.4	7.9
19	KI 4119	2.757	0.002	1.250	0.000	0.010	0.001	0.236	0.644	0.073	nd	4.975	26.8	24.8	67.6	7.7
20	KI 4079	2.834	0.002	1.170	0.001	0.008	0.000	0.131	0.645	0.190	0.016	4.996	16.9	13.6	66.7	19.7
21	KI 4061	2.794	0.003	1.210	0.001	0.011	0.001	0.169	0.644	0.141	0.018	4.990	20.8	17.7	67.5	14.8
22	KI 4081	2.870	0.002	1.135	0.001	0.014	0.001	0.092	0.566	0.275	0.025	4.980	14.0	9.8	60.7	29.5
23	KI 3001	2.861	0.000	1.129	0.002	0.005	0.000	0.083	0.626	0.317	0.023	5.045	11.7	8.1	61.0	30.9
24	KI 4106	2.855	0.001	1.144	0.001	0.008	0.000	0.134	0.543	0.273	0.022	4.980	19.7	14.1	57.2	28.7
25	KI 4076	2.878	0.002	1.130	0.001	0.007	0.000	0.079	0.567	0.304	0.023	4.991	12.3	8.4	59.7	32.0
26	KI 3381	2.833	0.001	1.164	0.000	0.007	0.001	0.126	0.644	0.227	0.018	5.020	16.4	12.7	64.5	22.8
27	KI 4110	2.880	0.001	1.135	0.001	0.007	0.000	0.094	0.503	0.319	0.021	4.961	15.8	10.3	54.9	34.8
28	KI 4063	2.827	0.002	1.179	0.001	0.007	0.001	0.139	0.589	0.227	0.018	4.989	19.1	14.5	61.7	23.8
29	KI 4104	2.855	0.001	1.149	0.001	0.006	0.000	0.108	0.572	0.286	0.021	4.999	15.9	11.2	59.2	29.6
												AVG	5.001			

Note: 0\* means <0.001; nd\* Ba not determined.

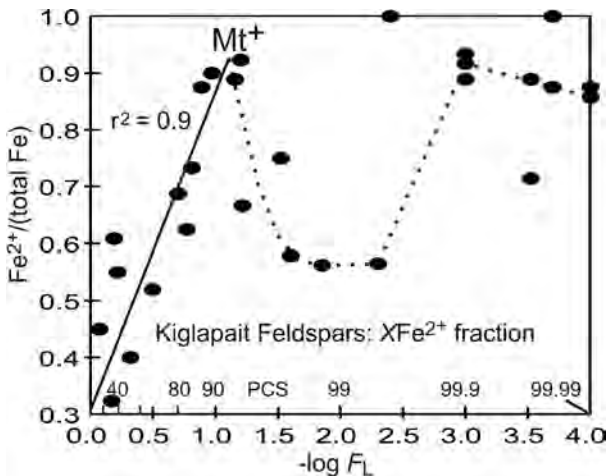


**FIGURE 4.** Stratigraphic plot of the ferrous/(ferric + ferrous) fraction in the analyzed feldspars, using the ferrous and ferric iron data from Table 2. The Y axis represents the ferrous fraction. There is a steady rise in  $Fe^{2+}$  through the Lower Zone (0–84 PCS) and Upper Zone to a ratio of >0.9 at 94 PCS, the stratigraphic level of the Main Ore Band. Here the ferric ratio increases, so the proportion of ferrous iron decreases to a minimum near a ratio of 0.58, thereafter rising again to ~0.9 with large individual variations near the end of crystallization.

porosity (Morse 1979, 2012, 2013). An exception occurs in the region 0–15 PCS where many low values of An may reflect injections of evolved magma. The low slope of the main trend in the Lower Zone is evaluated as reflecting the low silica activity in the troctolitic magma (Morse 2014).

The scatter of data at values beyond 99.5 PCS illustrates

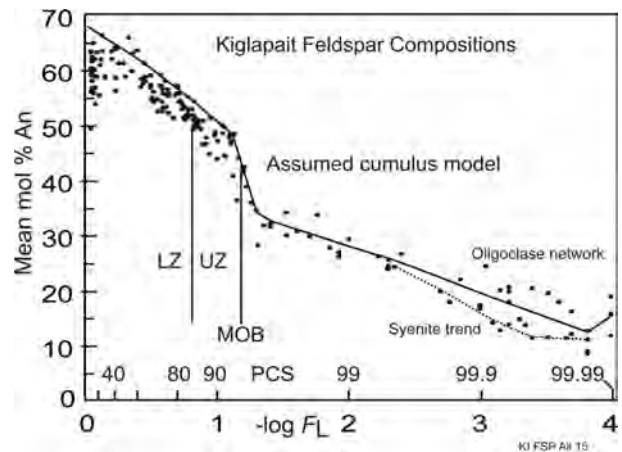


**FIGURE 5.** Stratigraphic plot of mean Kiglapait feldspar compositions determined by electron microprobe analysis in grain mounts. The Lower Zone–Upper Zone boundary is indicated at 84 PCS. MOB, Main Ore Band at 93.5 PCS;  $Ap^+$  occurs at 94 PCS. The “Syenite Trend” refers to the assumed path of crystals following the evolving liquid, whereas the “Oligoclase network” is interpreted to be the result of feldspar networks in the liquid structure (Philpotts et al. 1999) plus physically suspended oligoclase crystals.

the late increase in the An range with fractionation progress. It is interpreted as a sharp rise in the residual porosity owing to the presence of the increasingly important feldspar network in the liquid as discussed in Morse (2012) following Philpotts et al. (1999). The higher values of An come from distinctively albite-twinned crystals of oligoclase, some of which are partially resorbed. The lower values (dotted line) constitute a syenite trend

with fewer oligoclase networks.

Strongly reversed rims, adding as much as 32 mol% An above the mean, occur on plagioclase grains in Kiglapait troctolites and olivine gabbros (Morse and Nolan 1984). They are ubiquitous in these rocks, but minor in volume. They are attributed to effects of trapped liquid containing elevated Ca+Al from the augite component of the melt phase. They are remarkable particularly for preserving strong potassium and K/Na gradients throughout a long subsolidus cooling history. This feature requires that the K substitution in calcic plagioclase is linked to the tetrahedral Al/Si distribution, not to a simple K-Na exchange (Morse 1984).

### Ternary plots

The wet chemical data set and the original set of electron microprobe data are shown in the ternary plot of Figure 6 where they are keyed to the stages of the Upper Zone. The electron microprobe data plot exactly with the bulk composition data from wet chemical analyses until they begin to deviate after the appearance of apatite, where the electron microprobe data bifurcate into two trends: an oligoclase trend toward albite and a very scattered and thinly populated ternary array that leads to a dense population of mesoperthites in stratigraphic stage “f”. The oligoclase-albite array is the low-temperature exsolution trend with conjugate perthite seen in a cluster near Or<sub>50</sub> and having very

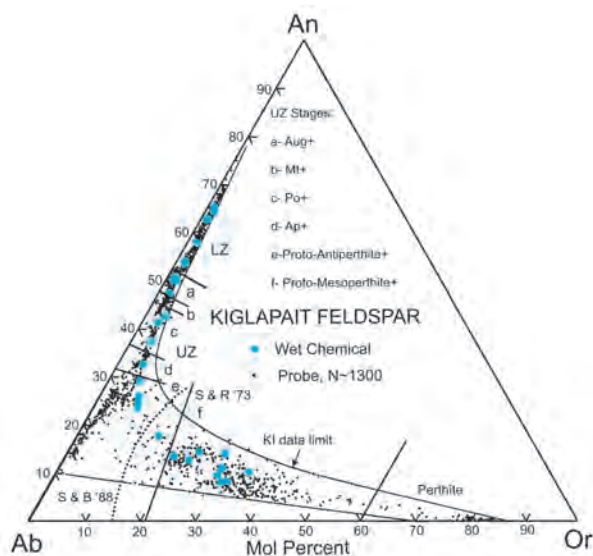


**FIGURE 6.** Ternary plot of Kiglapait feldspar compositions: large filled circles for wet chemical bulk analyses; small dots for mean electron microprobe analyses on 10 or more cleavage flakes in grain mounts. The stratigraphic stages are indicated as listed. The electron microprobe analyses fill the space among the bulk analyses until  $\sim$ An<sub>35</sub>, beyond which there is a separate oligoclase trend for the host crystals of antiperthite and mesoperthite, for which the unmixed and rare Or phase was generally missed in the microprobe analyses. The boundary of “Mesoperthite+” is drawn in a solid line from Speer and Ribbe (“S&R ’73”) and the petrographic data; a curved boundary shown as a dotted line (Smith and Brown 1988) does not comport as well with the Kiglapait petrographic data. Their perthite boundary is shown at Or<sub>60</sub>. Of special interest is the nearly An-free cluster near Or<sub>77-85</sub>, representing the exsolved perthite. (Color online).

low An contents. The other dots are in part (where near the wet chemical data) bulk compositions and in part variable mixtures of phases in the grain mounts on cleavage flakes.

In this figure the boundary between antiperthite and mesoperthite is taken from Speer and Ribbe (1973) and continued examination of the natural Kiglapait feldspars, using the protocol of extending it toward the An corner. A curved boundary (Smith and Brown 1988, Fig. 9.3) is shown dotted but does not comport with the Kiglapait observations. The Smith and Brown boundary of perthite from mesoperthite is also shown here as a slope with constant OR starting from Or<sub>60</sub>.

In the following section, uppercase AN and OR refer to the ternary fraction of those components, whereas An and Or are those compositions projected to the binaries.

The wet chemical compositions are shown by themselves with serial numbers in Supplementary<sup>1</sup> Figure S1, so that each one can be related to its composition in Table 1. Here the stratigraphic notations are retained, and the fields of proto-antiperthite and proto-mesoperthite are identified as being separated by the triclinic–monoclinic field boundary as found by Speer and Ribbe (1973). A detailed view of the combined wet chemical and electron probe analyses near the Ab corner is shown in Figure 7, along with sample numbers. The textually important samples KI 4075 and KI 3010 are also shown in black with their probe analyses. The important compositions of KI 4077 and 4078 have been added as calculated and adjusted from their whole-rock analyses (Morse 1981b) as described in Appendix<sup>1</sup> Table A2.

Samples KI 3010 and KI 4079 contain mesoperthite, whereas the more sodic KI 4061 does not, hence the mesoperthite limit is well defined for this data set. The position of the experimental Kiglapait endpoint is shown by a black cross near sample KI 4104 (99.99 PCS and therefore technically in the Upper Border Zone).

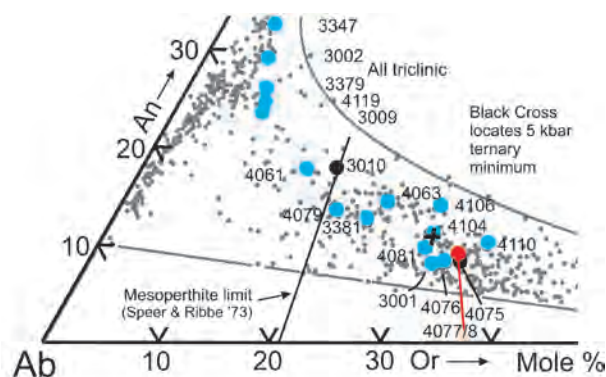


**FIGURE 7.** Ab corner of the ternary feldspar system with a key to the analysis numbers in Tables 1 and 2. The (heavy line) boundary between antiperthite and mesoperthite is taken from Speer and Ribbe (1973) running from Or<sub>21</sub> on a line to the An corner. Another arbitrary boundary between these two regions is preferred by some mineralogists as running from the Ab corner to 1:1 An:Or but not shown here. The mean composition of the uppermost samples KI 4077 + 4078 is shown near the lower right corner. A black cross near sample 4104 locates the endpoint of inferred last liquid. (Color online).

### Textural features

Six photomicrographs of late-stage mesoperthite and other intergrowths are shown in Figures 8 and 9. The first three of these in Figure 8 show a range of exsolution textures from a single sample, KI 3010. The fourth shows the singular ragged boundaries of relatively large feldspars found in some samples. Figure 9a shows a distinctive mesoperthite with small brown plates of ilmenite, and Figure 9b shows a characteristic image of coarse symplectite replacing mesoperthite.

### Occurrence of mesoperthites and symplectites

Most Kiglapait samples at and above 99.86 PCS contain mesoperthite exsolved from a monoclinic parental sanidine that was rich in sodium (Speer and Ribbe 1973). Of the 36 samples in this group, four have little or no mesoperthite. Four samples at the stratigraphic top of the group are assigned the PCS value 99.99, which is reserved for sandwich horizon rocks that are assigned to the Upper Border Zone. In some samples, coarse symplectites of orthoclase and oligoclase have replaced parts or all of the mesoperthites. The first of these symplectites occurs in trace amounts in sample KI 4081 at 99.94 PCS (Fig. 8), but the first robust example occurs at 99.95 PCS in sample KI 4108. Stratigraphically above this level are 19 samples among which 12 contain some amount of symplectite and of which 9 contain robust quantities. Nearly total reaction is observed in sample

KI 4104 (99.99 PCS), a sample that uniquely contains a 3 cm scale apatite crystal. This sample is featured in the last frame of a photomicrograph in Morse (2015b, Fig. 13.18).

### Composition of Kiglapait feldspar symplectites

The word symplectite was coined by Naumann in 1850 to describe a texture intimately involving two minerals such as those found in pegmatites (Johannsen 1939). An example from the Kiglapait alkali feldspars is shown from KI 4106 in Figure 9b. A nearby sample, KI 4108, contains large subhedral grains of extremely finely exsolved (~2  $\mu\text{m}$ ) mesoperthite with many mafic minerals and no symplectite.

It is of great interest to understand whether or not these symplectites have the same bulk composition as their host mesoperthites. Figure 10 shows a cluster of four samples studied in polished thin section, KI 4075, 4076, 4081, and 4110 (see also Fig. 7), for which the bulk compositions group on a tieline near OR 33 AB 59 AN 8 (ternary notation). A fifth sample, KI 4079 from 99.9 PCS, illustrates the feldspar trend from antiperthite toward Or-rich mesoperthite. The exsolved compositions in Figure 10 are from sample KI 4075. Exsolved oligoclase end-members group closely at the left end of the tieline, and the conjugate orthoclase compositions are scattered at the right end near Or<sub>80</sub>-An<sub>0</sub>. The symplectites have the same bulk composition as the resident mesoperthites. These features define a coarsening reaction (Smith and Brown 1988) in which the intrinsic strain of the coherent solvus is broken isocompositionally to yield the higher-temperature, strain-free solvus for which the local system is energetically minimized.

Such symplectite intergrowths have also been ascribed to the effects of low-temperature hydrothermal alteration near or below 300 °C, especially if they are turbid (e.g., Smith and Brown 1988). The Kiglapait symplectites are not turbid. Their textural relations, combined with wormy boundaries, suggest

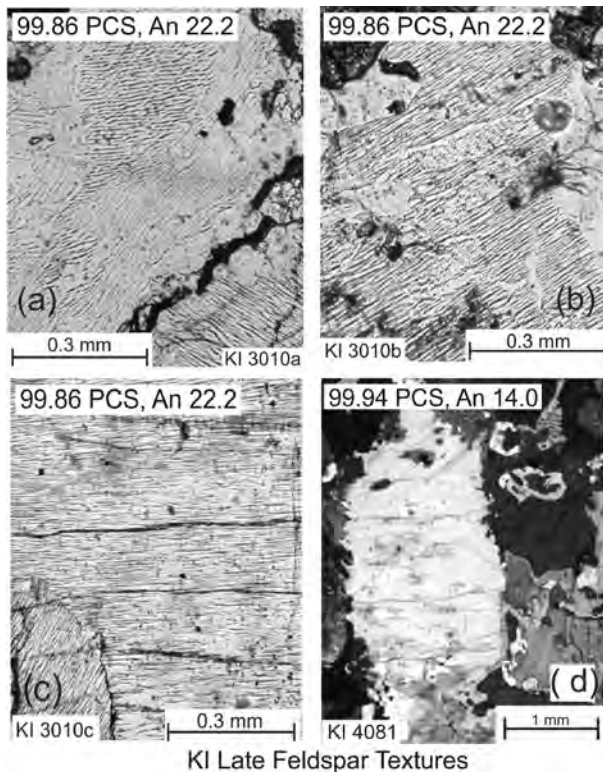
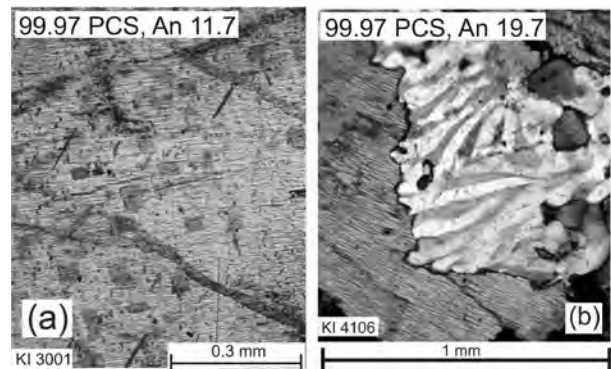


**FIGURE 8.** Photomicrographs. (a–c) Three examples of mesoperthite in one sample, all to scale, from variably oriented in a, to patchy in b, and well developed in c. (d) A large crystal of low-An mesoperthite with vermicular boundaries against all mafic phases, chiefly ferrohedenbergite, also accompanied by a coarser two-feldspar intergrowth (symplectite).



**Mesoperthite and arrested symplectite**

**FIGURE 9.** Photomicrographs of (a) mesoperthite typically containing very thin, equant exsolution plates of ilmenite, shown here as darker gray but pale brown in ordinary light. (All the Kiglapait feldspars are medium to dark gray in hand specimen and contain microscopic oriented mafic inclusions exsolved from the parent on slow cooling.) This is the sample for which the binodal solvus was determined in Morse (1969b). (b) Coarse symplectite of oligoclase (bright white) and orthoclase invading finely exsolved mesoperthite. The symplectite and mesoperthite have the same bulk composition.

a grain-boundary avenue of access (Fig. 9b). They suggest high-temperature effects in an isochemical reaction in terms of major components. From the singular association of extreme symplectite growth and coarse apatite shown in sample KI 4104, it may be inferred that the agent for this coarsening process was a vapor rich in fluorine. The temperature range of symplectite exsolution can be estimated from the solvus relationships, to be described below.

**EXPERIMENTAL METHODS**

The initial experimental study of the Kiglapait intrusion was the determination of the solvus of a Kiglapait mesoperthite (KI 3001) in platinum tubes over several months in cold-seal pressure vessels (Morse 1969b and discussed below). That was also the end of such experiments because the iron in rock compositions alloys with platinum, creating a serious container problem for rock compositions with mafic minerals. The container problem was eventually resolved by using graphite capsules in piston-cylinder apparatus in a new experimental program to determine the line of descent for the Kiglapait Lower Zone liquid at 5 kbar (Morse et al. 2004). Bulk compositions of finely ground Kiglapait minerals were made up from mineral powders to follow the olivine-plagioclase cotectic from nearly augite-free troctolite to saturation with augite. A previous study by Peterson (1999) on Upper Zone whole-rock compositions used the same experimental methods performed on a suite of variably evolved Upper Zone rock powders. The combination of the two studies provides a complete liquid line of descent for the intrusion. The liquid compositions are projected into the feldspar ternary in Figure 11. In this figure, the experimental feldspar compositions are shown as black diamonds and the coexisting melts in large red (grayscale) circles. The most Ab-rich black diamonds reflect the original experiments at 5 kbar. These were converted to representative values at 3 kbar (grayscale) as follows.

Pressure has a strong effect on plagioclase compositions because of the very different pressure effects of An and Ab on the melting temperatures. In the range 0–5 kbar albite melts at about 17 °C/kbar (Lange 2003), whereas anorthite melts at about 2.8 °C/kbar (Goldsmith 1980). The 5 kbar experimental data are therefore richer in An than the appropriate 3 kbar samples. Calculating these effects for An values in the region An = 20–30 yields results that vary depending on the loop-width (and hence  $K_D$ ; Morse 2015a) that is chosen. For likely realistic values of  $K_D$  near 0.5 the estimates yield corrections of –7 to –8 mol% An from the 5 kbar data to the 2.8 kbar data. Choosing the lowest of these corrections, the 2.8 kbar data for the three most Ab-rich feldspars in the diagram of Figure 11 fall on or near the liquid line of descent in such a way as to make credible tangents to the liquid path, as they must to represent differentiation faithfully. The results are shown in Figure 11 as gray diamonds.

Drill sample KI 4077, when melted at 5 kbar, yielded Or-rich crystals in a mesoperthite liquid composition. This result closely brackets the final melt composition at 5 kbar. The Appendix<sup>1</sup> to this paper provides the details of experimental studies bearing on the end of Kiglapait crystallization. It traces the sources leading

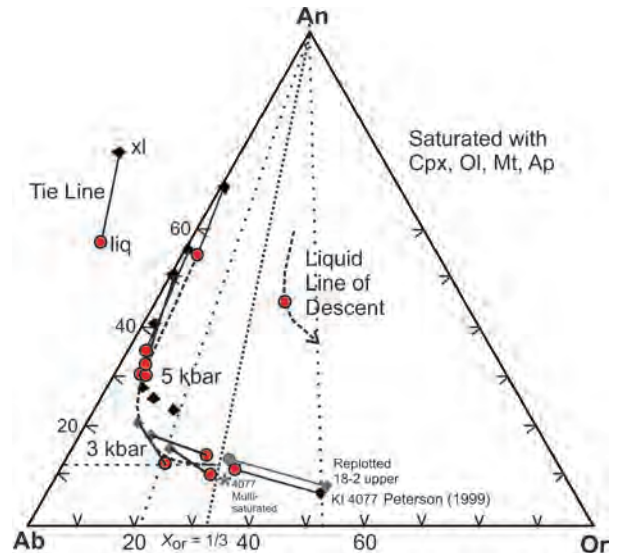
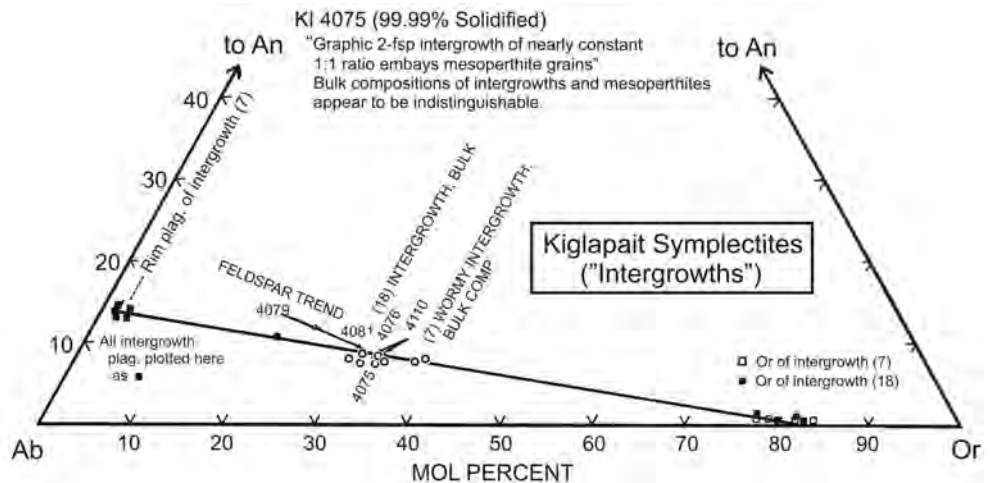


**FIGURE 11.** Ternary feldspar diagram showing 5 kbar experimental crystal-liquid tielines from Peterson (1999) in the Upper Zone and Morse et al. (2004) in the Lower Zone. The data are consistent with an invariant point at  $Or_{33}, An_{11}$  as shown by the intersecting dotted and dashed lines. In the lower left corner, the three black 5 kbar observations are corrected to the grayscale 3 kbar equivalents as discussed in the text. The grayscale tielines and points are re-plotted from Peterson’s tables and a multi-saturated melt composition (asterisk) is newly plotted from the Peterson data tables. Further descriptions can be found in the Appendix to this paper. The coarsely dotted lines from the An apex define the closest feldspar bracket about the 1/3 line with values of  $\sim Or_{20}$  and  $Or_{52}$ . (Color online.)

up to the work of Peterson, and describes the sample population in some detail. The critical sample numbers and their distribution are displayed in Figure 7, where they include samples KI 4077 and 4078 and help to define the end of crystallization. The Peterson plot of results from KI 4077 furnishes the Or tieline in the Peterson thesis. Using the original data, a recalculation of the experiment 18-2 data gave a slightly more An-rich and slightly longer tie line, shown in grayscale in Figure 11. Peterson’s tables also gave a glass composition for experiment 17-2 that was multiply saturated in feldspar, fayalite, and Cpx. The glass composition from this experiment is plotted as an asterisk in grayscale in Figure 11

► **FIGURE 10.** Microprobe analyses of five mesoperthite samples including KI 4075, which shows intergrowths of symplectite that embay mesoperthite grains. The bulk compositions of intergrowths (7) and (18) lie within the mesoperthite region at  $An_{10}$ . The plagioclase compositions of the intergrowths plot at about  $An_{15}$  with little Or. The corresponding Or-rich end-members cluster near  $Or_{80}$  and have very low An contents. The symplectitic intergrowths and the mesoperthites have bulk compositions that are essentially indistinguishable.



bit lower in An than the other experimental samples. Between the Ab-rich glasses and those from sample KI 4077, the final liquid composition of the intrusion is bracketed about  $X_{Or} = 1/3$ , but it is also not significantly different from the  $P$ - $T$  consolute line of Fuhrman and Lindsley (1988; see Fig. A-1 in the Appendix<sup>1</sup>).

## END OF KIGLAPAIT CRYSTALLIZATION: SOLIDUS–SOLVUS RELATIONS

### Nature of the Ab–Or solvus

The three major kinds of solvus are binodal, spinodal, and coherent, as discussed in Waldbaum and Thompson (1969) and reviewed in Morse (1994). The binodal and spinodal solvi meet at the critical point, and the spinodal lies everywhere else inside the binodal. The coherent solvus lies everywhere inside the spinodal, with a crest much lower than the others (e.g., Yund and Davidson 1978). It takes account of the strain energy developed at the physical interface between two intergrown (cohering) phases. The finely exsolved mesoperthite texture is metastably locked in place at room temperature because of its strong coherence. It is probable that the coherent solvus involves optimal phase boundaries (Bollmann and Nissen 1968). In the following discussion, the main focus is on the nature of the binodal solvus.

In the system Ab–Or there is an elegant calculation using Margules parameters of the Ab–Or solvus by Thompson and Waldbaum (1969), based on experimental results by two groups. Their Figure 13 shows a calculated solvus at 2 kbar with data points and a consolute (crest, critical) temperature  $T_c$  of 675 °C and a lower limit of 400 °C. The authors find a critical (consolute) composition of exactly  $X_{Or} = 1/3$ , and provide (in Waldbaum and Thompson 1969) a thermal scale of corresponding states for any pressure; in effect, the geometry of the solvus does not change if (as shown) the critical line is linear in  $P$ - $T$ - $N$  space ( $N$  = composition).

In a companion study from glass compositions at 5 kbar, Morse (1970) showed (in his Fig. 6) a solvus with  $T_c = 730$  °C, obtained from new data and with Margules parameters calculated by David Waldbaum. When these two solvi at 2 and 5 kbar are overlain and stretched so as to have the same critical points, they are essentially identical in shape, and retain the criterion of  $X_{Or} = 1/3$ . Examples of four compared solvi are shown in Figures S3–S4 in the Supplementary<sup>1</sup> Material to this paper.

### Ternary solvus properties: The system Ab–An–Or

The binodal solvus of a Kiglapait mesoperthite (KI 3001, Serial No. 23 in Table 1) from 99.97 PCS was determined at 0.5 kbar in sealed platinum tubes in externally heated cold-seal pressure vessels (Morse 1969b). Run times of 28 to 61 days provided constraints on the shape of the solvus, and  $T_c = 920$  °C; once again, the consolute composition is at  $X_{Or} = 1/3$ . Shorter runs revealed melting beginning at 925 °C. The limb compositions of the solvus were determined by X-ray diffraction. This solvus determination furnishes a useful starting point for the discussion of the natural solvus at ambient conditions (3 kbar, 1000 °C eutectic) at the end of crystallization. The results of this experiment are of special interest because the sample is a ternary feldspar with about 8% AN, hence more relevant to natural rocks than results in the binary system Ab–Or. When compared to the Ab–Or results discussed above, the Or limb is essentially indistinguishable, but the Ab limb becomes more Ab-rich than Ab–Or with lower temperature. This deviation can perhaps be ascribed to the effect of An on the system, making

the solvus somewhat wider at lower temperature: but see below!

In another comparison, the binary Ab–Or solvus of Hovis et al. (1991) is similar to the mesoperthite solvus when adjusted to the same temperature interval. In fact, it *perfectly matches along the Ab limb*, but the Hovis et al. Or limb is somewhat more potassic than the Kiglapait result, yielding a somewhat wider solvus in the other direction (Fig. S5<sup>1</sup>). The hydrous 0.5 kbar binodal solvus with a crest at 920 °C of the Kiglapait mesoperthite KI 3001 (Morse 1969b) was cited by Fuhrman and Lindsley (1988) as essentially fitting their ternary (An–Ab–Or) thermal model at 900 °C, 0.5 kbar.

### The multicomponent system: Solvus for feldspars saturated with mafic components

The experimental data from the Kiglapait intrusion are the most pertinent to the investigation at hand. Accordingly, we begin with the shape and consolute point of the experimental solvus.

Sample KI 3001 (Figs. 7 and 9a) at AN = 8 is lowest in the range of the AN values for Kiglapait mesoperthites. From the cluster of samples in Figure 7, sample KI 4104 at AN 11 is more central among the mesoperthites and will serve as more representative of the array. This AN value can be used as a proxy for finding the relevant critical point of the inferred Kiglapait solvus. To do this, we shall need adjustments for bulk composition, pressure, and Ba content.

Adjustments for  $P$  and  $X$  can be conveniently and appropriately made from the “plutonic pairs” data of Table 3 in Fuhrman and Lindsley (1988). From their 3 kbar data, we find a compositional correction for temperature of +12.83 °C per unit of AN. (The temperature difference is 989 – 921 = 68 °C; the compositional difference is 5.3 AN units.)

For the Kiglapait case there is no pressure correction if we choose the Fuhrman–Lindsley value of 989 °C at 3 kbar and AN = 10. For AN = 11 therefore we have  $T = 989 + 13 = 1002$  °C. The same source suggests an addition of +20 °C for the mole fraction of celsian (Cn) = 0.02 and sample 4104 has 0.023 Cn, so adding 20 °C we arrive at 1022 °C for the consolute temperature at 3 kbar for sample KI 4104.

But the experimentally derived temperature at the end of crystallization at 3 kbar (Morse and Brady 2017a) is 1000 °C, so the solvus crest is 22 °C higher, and the solidus and solvus have intersected. Recalling Figure 11, the opposing tie lines have considerable length, meaning that they define the limbs of the solvus. We now plot the two opposing tie line lengths at 0.2 and 0.52  $X_{Or}$  (see dotted lines in Fig. 11) to form the isotherm connecting the two solvus limbs most closely bracketing the eutectic. The effect of pressure from 5 to 3 kbar would be to widen the melting loops. This is effectively done already because the opposing liquid compositions in Figure 11 bracket the liquid composition at  $X_{Or} = 1/3$  but do not quite reach it. The solvus needs to be raised to fit the crystal + liquid brackets. In this operation the solvus is raised by 25 °C from 1022 °C to a metastable consolute temperature of 1047 °C. The result meets both sides of the experimental results, as shown in Figure 12.

### Experimental phase equilibria for Figure 11

The experimental tie lines of Peterson (1999) define loop widths and thus values of  $K_D$  (e.g., Morse 2000) at the 3 kbar solidus temperature of 1000 °C. The tie lines appear in Figure 11

centered on  $X_{Or} = 1/3$ . Their  $K_D$  values are 0.540 for the Ab loop and 0.473 for the wider Or loop. The solidus curves in Figure 12 have been drawn arbitrarily and the liquidus curves added via the two values of  $K_D$  cited here. The linear partitioning equation is  $D = K_D \cdot X_2^2 + X_1^2$ , where  $D$  is the partition coefficient set  $\leq 1.0$ ,  $K_D$  is the exchange coefficient,  $X$  is a mole fraction, 1 is the low-temperature melting component, and 2 is the high-temperature melting component. Solving for the liquid composition,  $X_1^L = X_1^S/D$ . The limiting solidus temperatures are as yet provisional, but could easily be determined from experiment.

### Thermal history of the symplectites

The electron probe data combined with the bulk compositions determined by wet chemistry show that the coarse symplectites replacing mesoperthite (e.g., Fig. 9b) have the same bulk composition as the mesoperthites (Fig. 10). They are exsolved to extreme compositions at oligoclase and orthoclase. The relevant compositions projected to the Ab-Or join are  $Or_{33}$ ,  $\sim Or_{33}$ , and  $Or_{80\pm 3}$ . When these compositions are plotted on the solvus limbs extended down-temperature from Figure 12 (see Fig. S2

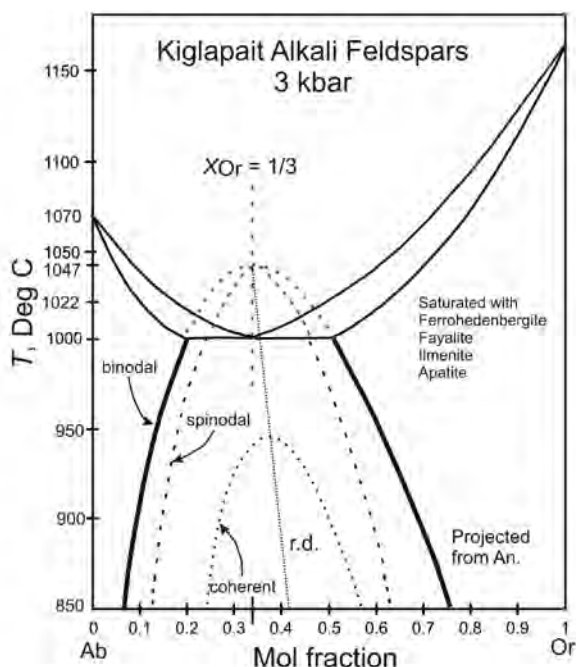


**FIGURE 12.** Liquidus, solidus, and solvus of the Kiglapait alkali feldspars adjusted to 3 kbar. The projected Ab-Or azeotrope is generated using linear partitioning (Morse 2000) from the tielines of Figure 11 and the loops of Waldbaum and Thompson (1969). The binodal is generated from experiments by Morse (1969b, 1970) adjusted for temperature and Ba content from Fuhrman and Lindsley (1988) as described in the text. The eutectic temperature at 1000 °C is experimental from studies of the solidus of samples KI 4077 and 4078 (Morse and Brady 2017a). The spinodal is estimated from Waldbaum and Thompson (1969). The coherent solvus (dotted) is estimated from Yund and Davidson (1978). The dotted center line is the rectilinear diameter, r.d. The liquidus experiments of Figure 11 require that the solidus and solvus are embedded. The endpoint temperatures at Ab and Or are provisional. Variations on this diagram are included in the Supplementary Material<sup>1</sup> to this paper.

in Supplementary Material<sup>1</sup>), they record the final temperature of exsolution. Essentially all the significant compositional variation occurs in the orthoclase limb. The resulting mean closure temperature is 795 °C, with a maximum of 830 °C and a minimum of 758 °C. The cooling path extends  $205 \pm 36$  °C below the solidus.

The agent of coarsening is presumably a vapor phase in equilibrium with apatite and hence rich in fluorine. In most cases, the coarsening continues to an exhaustion of the assumed vapor. Some samples, as in KI 4104, are completely reacted to symplectite and this one contains a large apatite crystal.

Any hypothesis of late hydrous alteration at low temperatures to make the Kiglapait symplectites from mesoperthite is falsified by the high closure temperature. The estimated solvus and the well-characterized compositions of the exsolved symplectite pairs on the solvus limbs provide a realistic thermal history for a dry ferrosyenite at moderate crustal pressures.

## PHASE RELATIONS

### Effect of pyroxene on feldspar composition

The last liquid to crystallize in the Kiglapait intrusion may be considered that of the last rock, KI 4078 (composition given in Morse 1981b). This rock contains 7.14% CaO and 10.6%  $Al_2O_3$ . The oxygen norm contains 63.5% feldspar with composition An 10.9. The rock (liquid) sample has in its oxygen norm 30% Augite (here actually ferrohedenbergite).

The coexisting pyroxene in this rock=liquid (Morse and Ross 2004) has the composition 17.75% CaO and 1.23% alumina. Thirty percent of 17.75 is a total of 5.33 CaO contributed by the pyroxene. Without the presence of this 30% normative pyroxene, the rock=liquid composition would have approximately  $7.14 - 5.33 = 1.81\%$  CaO. It is therefore safe to say that the activity of CaO in the liquid is due in large part to the pyroxene component of the bulk composition.

At equilibrium, the activities of Ca and Al are equal in the liquid, feldspar, and pyroxene, and their combined presence dictates the final feldspar composition. Without the presence of the pyroxene, the feldspar would be lower in the An component. Saturation of the melt with calcic aluminous pyroxene at high temperature (1000 °C) dictates the relatively An-rich composition of the final Kiglapait liquid and feldspar.

### Phase rule variance

Because the endpoint of Kiglapait crystallization occurs at a 3 kbar eutectic as determined by experiment to be the beginning of melting (Morse and Brady 2017a), it is appropriate to enumerate the components and phases required to make the system invariant. The eutectic is the lowest melting point of a system. For the Gibbs phase rule we may write

$$W = c + 2 - \varphi \quad (1)$$

where  $W$  is the variance,  $c$  is the number of components, and  $\varphi$  is the number of phases. We have already specified that  $P$  and  $T$  are invariant at 3 kbar and 1000 °C, so now  $W = c - \varphi$  and for invariance, the number of components and the number of phases must be equal. This justification is here reported in Table 3 for the uppermost sample KI 4078. Note that this is an Mg-free system. The ferric iron is shared by the pyroxene as well as rare magnetite.

## COMPARISONS TO OTHER SYENITES

## The Gardar Province

The combination of ferrohedenbergite and syenite is, of course, not unique to the Kiglapait intrusion. The Gardar Province of southwest Greenland has considerable affinities with coastal Labrador and is prolific with syenites and gabbros that are in general somewhat younger and more alkalic than the intrusive rocks of the Nain Province. Of these, the Klokken complex (Parsons 1979; Parsons and Brown 1988; Upton 2013) is of interest. It contains a syenite surrounded by a gabbro unit. The plagioclase composition ranges from An<sub>53</sub> in syenogabbro through alkali feldspars that lie well within the two-feldspar field of Tuttle and Bowen (1958), and eventually evolve to a low-An cluster at Or<sub>38</sub>. The ferrohedenbergite composition reaches ~95% of the Fe end-member but is then joined by acmite and alkali amphiboles. The amount of K<sub>2</sub>O in the main Klokken syenodiorite sheet is 2.6% (Parsons 1979); in the Kiglapait parent magma it is an order of magnitude lower, 0.22–0.29% (Morse 2015b, Table 13.2). The Klokken system is hydrous and alkalic, at an estimated pressure near 1 kbar, and hence quite unlike the dry Kiglapait ferrosyenite at 3 kbar.

## The Sybille Monzosyenite

Like the Kiglapait intrusion, the Sybille intrusion is related to a major anorthosite complex, the Laramie Anorthosite Complex of Wyoming (Fuhrman et al. 1988). Here the plagioclase composition is less varied (An<sub>45</sub>–An<sub>25</sub>) but the olivine closely approaches pure fayalite and the later feldspars are mesoperthites. The inferred magmatic temperatures at 3 kbar are in the range 950–1050 °C and the oxygen fugacity of crystallization is estimated at ~FMQ-1.5 to -2.0 log units, somewhat lower than the FMQ-1 estimated for the Kiglapait syenites (Morse 1980, Fig. 10). The authors note the occurrence of graphite and CO<sub>2</sub>-rich fluid inclusions suggesting the presence of a vapor phase. These compositions and equilibria are much closer to the inferred Kiglapait conditions than those at Klokken.

## CONCLUDING REMARKS

The solvus determinations of the 1969–1970 era all appear to have  $X_{Or} = 1/3$  and remain relevant to the multicomponent system of the Kiglapait syenites. The 1969 solvus has a widening that can be ascribed to its An content. The Ca, Al components of the Kiglapait ferroan augite series have demonstrable capacities for exchange and equilibrium with alkali feldspars. This capacity generates a relatively An-rich multiphase eutectic at high temperature and pressure. The bracketing melting experiments at the end of crystallization quantify the interaction of solidus and solvus in an azeotrope.

It is strange indeed that the first experimental solvus determination on a natural An-bearing feldspar with water in 1968 should now play a central role in the calculation of a solvus that fits new experimental data in a multicomponent dry system at pressure. The capacity of this solvus to bracket the low-temperature conjugate limits of the symplectite solvus is a further valuable result.

Among other useful features of this study are the characterization of syenites derived from initially troctolitic melts that remain saturated with olivine even to the exhaustion of

TABLE 3. Kiglapait endpoint: Components and phases (Sample KI 4078)

Components	%	Special phase groups	Phases	Notes
SiO <sub>2</sub>	51.0		FSP 1	Ab rich
TiO <sub>2</sub>	1.8	ILM	FSP 2	Or rich
Al <sub>2</sub> O <sub>3</sub>	10.6	FSP + Cpx	Fa	Olivine
Fe <sub>2</sub> O <sub>3</sub>	3.1	Cpx	Cpx	Ferrohedenbergite
FeO+MnO	18.4	Cpx + ILM	Ilmenite	
CaO	7.2	Cpx + FSP	Magnetite	present in norm
Na <sub>2</sub> O	3.5	FSP1 + Cpx	Apatite	
K <sub>2</sub> O+BaO	3.4	FSP 2	Liquid	
P <sub>2</sub> O <sub>5</sub> +F	1.0	AP	Vapor	
	100.0			
	Nine		Nine	

Note: MgO = 0.

magnesium. The Kiglapait feldspar evolution differs from the wetter, more alkalic, and shallower Garder examples of syenite but has similarities to the dry and more reduced Sybille monzosyenite. The downward trend of the biotite mode to zero with reaction progress, along with the absence of amphibole, helps to define the dry nature of the magma. The origin of the symplectites involves no metasomatic change of composition and is therefore once again shown to be due to isocompositional coarsening, terminated locally at the exhaustion of a coarsening agent at equilibrium with the components of apatite.

## IMPLICATIONS

The long evolution of Kiglapait feldspars during fractionation has led to an unbroken sequence from An<sub>68</sub> to a systematic enrichment in Ab and Or, reaching a well-defined endpoint near  $X_{Or} = 1/3$ , AN 11 at the last liquid. This path includes the development of orthoclase patches in antiperthites and a subsequent progress to mesoperthite, which then encountered the binodal solvus and an azeotropic endpoint. Mesoperthite still exists abundantly in the rocks near the end of crystallization, but not at it. Instead, the last rocks to crystallize contain two feldspars, once joined azeotropically with melt, but now in various stages of subsolidus equilibration. It is noteworthy that the textural evidence of arrested dihedral angles of Cpx-Plag-Cpx as found in the smaller and cooler Rum and Skaergaard intrusions by Holness (2007) and Holness et al. (2007) are generally not present in the Kiglapait intrusion, where all such angles tend to be at the maximum of 120°, consistent with the long, slow cooling history of this large body of cumulates. This duration of evolution and cooling may not be unique among slowly cooled magma bodies at pressure, but it is uncommon. With this evolution the role of potassic feldspar is of particular importance, not least because of its demonstrated affinity for Sr and Ba (Morse and Allaz 2013). This affinity may have played a significant role in the observed but poorly understood fractionation of <sup>87</sup>Sr observed in the Kiglapait Upper Zone (Morse 1983).

## ACKNOWLEDGMENTS

My debt to the early team of Jim Thompson and Dave Waldbaum will be evident in the text; my sense of their loss is acute. Hatten Yoder was my host at the Geophysical Laboratory; Frank Schairer and Felix Chayes were my other tutors. My office mate was Ikuo Kushiro, and we discussed the structure of silicate melts. I am grateful to Abby Peterson for making such a valuable scientific contribution in her M.S. thesis. The XRF analyses for BaO in Table 1 were made in the UMASS XRF lab by Mike Vollinger. Demanding yet valuable reviews of an earlier version of the manuscript by Ian Parsons and Hanna Nekvasil are gratefully acknowledged. A welcome and rigorous review by Don Lindsley and another by James Scoates helped to focus the paper much more sharply. I thank Peter Robinson and Tony

Philpotts for helpful previews and comments. The much-tried patience and critical help of the Associate Editors is gratefully acknowledged. Funding: This paper is based upon research supported by the U.S. National Science Foundation under Award No. EAR 0948095.

## REFERENCES CITED

- Berg, J.H. (1977) Dry granulite mineral assemblages in the contact aureole of the Nain Complex, Labrador. *Contributions Mineralogy Petrology*, 64, 32–52.
- Berg, J.H., and Docka, J.A. (1983) Geothermometry in the Kiglapait aureole, Labrador. *American Journal of Science*, 283, 414–434.
- Bollmann, W., and Nissen, H.-U. (1968) A study of optimal phase boundaries: the case of exsolved alkali feldspars. *Acta Crystallographica*, A24, 546–557.
- Bowen, N.L. (1915) The crystallization of haplobasaltic, haplodioritic, and related magmas. *American Journal of Science*, 40, 161–185.
- (1945) Phase equilibria bearing on the origin and differentiation of alkaline rocks. *American Journal of Science*, 243a, 75–89.
- Goldsmith, J.R. (1980) Melting and breakdown reactions of anorthite at high pressures and temperatures. *American Mineralogist*, 65, 272–284.
- Fuhrman, M.L., and Lindsley, D.H. (1988) Ternary-feldspar modeling and thermometry. *American Mineralogist*, 73, 201–215.
- Fuhrman, M.L., Frost, B.R., and Lindsley, D.H. (1988) Crystallization conditions of the Sybille Monzosyenite, Laramie Anorthosite Complex, Wyoming. *Journal of Petrology*, 29, 699–729.
- Holness, M.B. (2007) Textural immaturity of cumulates as an indicator of magma chamber processes: infiltration and crystal accumulation in the Rum Eastern Layered Intrusion. *Journal of the Geological Society of London*, 164, 529–539.
- Holness, M.B., Tegner, C., Nielsen, T.F.D., Stripp, G., and Morse, S.A. (2007) A textural record of solidification and cooling in the Skaergaard Intrusion, East Greenland. *Journal of Petrology*, 48, 2359–2377.
- Hovis, G.L., Delbove, F., and Roll Bose, M. (1991) Gibbs energies and entropies of K-Na mixing for alkali feldspars from phase equilibrium data: Implications for feldspar solvi and short-range order. *American Mineralogist*, 76, 913–927.
- Huntington, H.D. (1979) Kiglapait mineralogy I: Apatite, biotite, and volatiles. *Journal of Petrology*, 20, 625–652.
- Johannesen, A. (1939) *A Descriptive Petrography of the Igneous Rocks*, 2nd ed., vol. 1. 318 pp. University of Chicago Press.
- Lange, R.A. (2003) The fusion curve of albite and the compressibility of NaAlSi<sub>3</sub>O<sub>8</sub> liquid with pressure. *American Mineralogist*, 68, 477–493.
- Morse, S.A. (1969a) The Kiglapait Layered Intrusion, Labrador. *Geological Society America Memoir* 112, 204 pp, doi: 10.1130/MEM112-p1.
- (1969b) Feldspars. *Carnegie Institution of Washington Year Book*, 67, 120–126.
- (1970) Alkali feldspars with water at 5 kb pressure. *Journal of Petrology*, 11, 221–251.
- (1978) Test of plagioclase dispersion method and rapid probe analysis. *American Mineralogist*, 63, 768–770.
- (1979) Kiglapait geochemistry II: Petrography. *Journal of Petrology*, 20, 591–624.
- (1980) Kiglapait mineralogy II: Fe-Ti oxide minerals and the activities of oxygen and silica. *Journal of Petrology*, 21, 685–719.
- (1981a) Kiglapait geochemistry III: Potassium and rubidium. *Geochimica et Cosmochimica Acta*, 45, 163–180.
- (1981b) Kiglapait geochemistry IV: The major elements. *Geochimica et Cosmochimica Acta*, 45, 461–479.
- (1983) Strontium isotope fractionation in the Kiglapait intrusion. *Science*, 220, 193–195.
- (1984) Cation diffusion in plagioclase feldspar. *Science*, 225, 504–505.
- (1994) *Basalts and Phase Diagrams*. Krieger, Florida, 493 pp.
- (1997) Binary solutions and the lever rule revisited. *Journal of Geology*, 105, 471–482.
- (2000) Linear partitioning in binary solutions. *Geochimica et Cosmochimica Acta*, 64, 2309–2319.
- (2012) Plagioclase An range and residual porosity in igneous cumulates of the Kiglapait Intrusion. *Journal of Petrology*, 53, 891–918.
- (2013) Solidification of trapped liquid in rocks and crystals. *American Mineralogist*, 98, 888–896.
- (2014) Plagioclase fractionation in troctolitic magma. *Journal of Petrology*, 55, 2403–2418.
- (2015a) Linear partitioning in binary solutions: A review with a novel partitioning array. *American Mineralogist*, 100, 1021–1032.
- (2015b) Kiglapait Intrusion, Labrador. In B. Charlier, O. Namur, R. Latypov, and C. Tegner, Eds., *Layered Intrusions*, p. 589–648. Springer.
- Morse, S.A., and Allaz, J. (2013) Experimental partitioning of Sr and Ba in Kiglapait feldspars. *American Mineralogist*, 98, 2197–2200.
- Morse, S.A., and Brady, J.B. (2017a) Thermal history of the Upper Zone of the Kiglapait intrusion. *Journal of Petrology*, in press.
- (2017b) The system fayalite-albite-anorthite and the syenite problem. *American Mineralogist*, 102, 2062–2068.
- Morse, S.A., and Nolan, K.M. (1984) Origin of strongly reversed rims on plagioclase in cumulates. *Earth and Planetary Science Letters*, 68, 485–498.
- Morse, S.A., and Ross, M. (2004) Kiglapait mineralogy IV: The augite series. *American Mineralogist*, 89, 1380–1395.
- Morse, S.A., Brady, J.B., and Sporleder, B.A. (2004) Experimental petrology of the Kiglapait intrusion: Cotectic trace for the Lower Zone at 5kb in graphite. *Journal of Petrology*, 45, 2225–2259.
- Nekvasil, H., and Lindsley, D.H. (1990) Termination of the 2 feldspar + liquid curve in the system Ab-Or-An-H<sub>2</sub>O at low H<sub>2</sub>O contents. *American Mineralogist*, 75, 1071–1079.
- Parsons, I. (1979) The Klokken gabbro-syenite complex, South Greenland: Cryptic variation and origin of inversely graded layering. *Journal of Petrology*, 20, 653–694.
- Parsons, I., and Brown, W.L. (1988) Sidewall crystallization in the Klokken intrusion: zoned ternary feldspars and coexisting minerals. *Contributions to Mineralogy and Petrology*, 98, 431–443.
- Parsons, I., Fitz Gerald, J.D., and Lee, M.R. (2015) Routine characterization and interpretation of complex alkali feldspar intergrowths. *American Mineralogist*, 100, 1277–1303.
- Peterson, A.L. (1999) Quest for the liquid line of descent of the Upper Zone of the Kiglapait intrusion, Labrador, Canada: an experimental study. M.S. thesis, University of Massachusetts, 80 pp.
- Philpotts, A.R., Brustman, C.M., Shi, J., Carlson, W.D., and Denison, C. (1999) Plagioclase chain networks in slowly cooled basalt magma. *American Mineralogist*, 84, 1819–1829.
- Ryan, A.B. (1990) Preliminary geological map of the Nain Plutonic Suite and surrounding rocks (Nain-Nutak, NTS 14 SW). Newfoundland Department of Mines and Energy, Geological Survey Branch, Map 90-44, scale 1:500,000.
- Smith, J.V., and Brown, W.L. (1988) *Feldspar Minerals: Volume 1: Crystal Structures, Physical, Chemical, and Microtextural Properties*. Springer-Verlag, Berlin-Heidelberg, 828 pp.
- Speer, J.A., and Ribbe, P.H. (1973) The feldspars of the Kiglapait intrusion, Labrador. *American Journal of Science* 273-A, 468–478.
- Sporleder, B.A. (1998) Liquid line of descent of the Lower Zone of the Kiglapait Intrusion, Labrador, Canada: An experimental study. M.S. thesis, University of Massachusetts, 93 pp.
- Stacey, F.D., and Davis, P.M. (2009) *Physics of the Earth*, 4th ed. Cambridge University Press, 532 p.
- Stewart, D.B., and Roseboom, E.H. Jr. (1962) Lower temperature termination of the three-phase region plagioclase-alkali feldspar-liquid. *Journal of Petrology*, 3, 280–315.
- Thompson, J.B. Jr., and Waldbaum, D.R. (1969) Mixing properties of sanidine crystalline solutions: III. Calculations based on two-phase data. *American Mineralogist*, 54, 811–838.
- Tuttle, O.F., and Bowen, N.L. (1958) Origin of granite in the light of experimental studies in the system NaAlSi<sub>3</sub>O<sub>8</sub>-KAlSi<sub>3</sub>O<sub>8</sub>-SiO<sub>2</sub>-H<sub>2</sub>O. *Geological Society of America Memoir*, 74, 153 pp.
- Upton, B.G.J. (2013) Tectono-magmatic evolution of the younger Gardar southern rift, South Greenland. *Geological Survey of Denmark and Greenland Bulletin* 29, 124 pp.
- Waldbaum, D.R., and Thompson, J.B. Jr. (1969) Mixing properties of sanidine crystalline solutions: IV. Phase diagrams from equations of state. *American Mineralogist*, 54, 1274–1298.
- Xue, S., and Morse, S.A. (1993) Geochemistry of the Nain massif anorthosite, Labrador: Magma diversity in five intrusions. *Geochimica et Cosmochimica Acta*, 57, 3925–3948.
- Yoder, H.S., Stewart, D.B., and Smith, J.R. (1957) Ternary feldspars. *Carnegie Institution of Washington Yearbook*, 56, 206–214.
- Yund, R.A., and Davidson, P. (1978) Kinetics of lamellar coarsening in cryptoperthites. *American Mineralogist*, 63, 470–477.

MANUSCRIPT RECEIVED FEBRUARY 3, 2017

MANUSCRIPT ACCEPTED MAY 27, 2017

MANUSCRIPT HANDLED BY CALVIN BARNES